CHARACTERISTICS OF AN INNOVATIVE PHOTOELECTRIC SENSOR DURING PERIODICAL FROST AND DEFROST CYCLES

W. Wang, associate professor, The Department of Building Environment and Facility Engineering, The College of Architecture and Civil Engineering, Beijing University of Technology, Beijing, China
J. Xiao, Master, China architecture design and research group, Beijing, China
Q.C. Guo, Master, The Department of Building Environment and Facility Engineering, The College of Architecture and Civil Engineering, Beijing University of Technology, Beijing, China
Y.H. Zhao, professor, The Department of Building Environment and Facility Engineering, The College of Architecture and Civil Engineering, Beijing University of Technology, Beijing, China

Abstract: Aiming to introduce photoelectric technique into practical application of defrost control for air source heat pump (ASHP), an innovative photoelectric sensor, referred to as "Tube Embraced Photoelectric Sensor" (TEPS), is presented in this paper. Experiments are carried out in a controlled environmental chamber. Ten TEPSs in different structural parameters are developed and installed on a commercial size air source heat pump, which has a nominal heating capacity of 60kW. The characteristics of TEPSs are experimentally investigated in 260min with 9 periodical frosting and defrosting cycles. Compared with the original defrost control strategy used by the manufacturer, experimental results demonstrate that TEPSs can substantially prolong defrost intervals from 28.8min to 52min under the experimental conditions, and the numbers of defrost cycles can be reduced from 9 to 5. This ensures the units to avoid frequent mal-defrost phenomena. Consequently, both the heating efficiency and COP of the test units can be improved up to 8.0%.

Keywords: heat pump, defrosting, COP, energy consumption

1 INTRODUCTION

Frost formation initiate when the heat exchanger surface temperature is below both the environmental dew point and freezing temperature. Frosting has both positive and negative effects. The roughness of the frost layer enlarges the heat transfer area and affects the boundary layer, improving local heat transfer. Frost also fills in the gaps between tubes and fins, which reduces the contact resistance. With the growth of frost, the area of air passage becomes narrowed, and then the local air flow rate increases. This improves the local heat transfer rate. Therefore, in some certain period at the beginning of frosting, heat transfer is enhanced. However, after this temporary period, the negative effects, such as blockage of the air passage, heat insulation effect, dominates the heat transfer process. With the increase of air side pressure drop and heat resistance of the frost layer, total heat transfer rate is actually reduced. Defrost cycles must be implemented to restore the original capacity of the evaporator and improve the energy efficiency of a refrigeration system or ASHP unit. To mimic the defrost initiation and termination schemes used by the manufacturer of the heat pump, (O'Neal et al. 1991) initiated a defrost cycle manually when the capacity of the heat pump dropped by 20% from its peak capacity (2.5tons) after a previous defrost. Defrost termination was also carried out manually when the temperature of the refrigerant exiting the bottom circuit of the outdoor coil rose above 65°F. Studied by (Lenic et al. 2009), the overall heat transfer coefficient decreased 17% when the average frost layer thickness reached 1.0mm.

Among various researches related to optimal defrost control strategy, the determination of defrosting initiation point is a hot topic. Many studies have focused on it, including artificial intelligence techniques (Datta and Tassou 1999), neural networks (Datta and Tassou 2002), air pressure difference (Heinzen 1988), temperature difference between air and evaporator surface (Ciricillo 1985), fan power sensor (Muller 1975), fiber optic sensors (Paone and Rossi 1991), comparing the heat transfer rate on the air and refrigerant side of the evaporator (Thybo et al. 2002), measuring the thermal conductivity of ice (Llewelyn 1984; Woodley 1989; Paone and Rossi 1991), and detecting the refrigerant flow instability (Lawrence and Evans 2008). However, none of the methods listed above can detect the frost growth directly in real-time. The monitored parameters for determining the frost growth are chosen either from the condition for frost formation, such as the temperature of ambient and heat exchanger, or the by-products of frosting, including the variations of air pressure difference, fan power and the refrigerant flow instability. Depending on these indirect parameters, current units always defrost on undesirable conditions, and mal-defrost operations often occur in practical application with two opposite phenomena. The first phenomenon happens in dry and cold climate regions, showing the unit defrosts while frost does not exist on the heat exchanger surface. The second phenomenon occurs in humid climate regions, showing the unit does not defrost even though the heat exchanger surface has been fully covered with frost. Ultimately, these mal-defrost operations lead to a large quantity of energy consuming and uncomfortable heating effect to the users. Therefore, to avoid units defrosting on undesirable occasions, technologies for detecting frost directly and accurately are required.

As reported by (Byun et al. 2006), (J. Xiao et al. 2009), photoelectric technology exhibits feasible and reliable characteristics to monitor the frost growth directly and timely. A photoelectric sensor is composed of an emitter and a receiver. Once driven with current via an electrical source, the emitter emits constant infrared rays to the receiver through a passage. Then the infrared energy can be absorbed and transformed into current by the receiver. In the occasion that no frost exists in the passage, most of the infrared energy can be absorbed by the receiver, the output voltage remains at its minimum value. With the accumulation of the frost, the infrared energy arriving at the receiver is weakened or interrupted, the output voltage increases correspondingly. Finally, when the passage is fully filled with frost, little infrared energy reaches the receiver, the output voltage gets its maximum value. In the study of (J. Xiao et al. 2009), three sections, namely the initial section, the respond section and the stable section and two properties, “on-off” and “linear”, are found to be the primary characteristics of the photoelectric technology. The “on-off” property can be specified as follows: output voltage 0V for “off” control, while 9V for “on” control. Based on this performance, the initiation point and stopping point for defrost control can be easily determined.

(Byun et al. 2006) evaluated the method of using photo-electric sensor by comparing its performance with conventional time control defrost system. The results indicated that overall heating capacity of photo-electric sensor detection method was 5.5% higher than that of time control method. And the most efficient initiation point of the defrost cycle was further investigated experimentally. In their study, since the diameter of a photo-electric sensor is 3mm, and the sensors are placed between fins, the fin spaces have to be enlarged to 4 FPC rather than the typical distance of 8-10 FPC. In addition, emitter and receiver of photo-coupler must be located on a line of sight. As the location of emitter and receiver deviated, the output voltage of receiver is deviated.

The purpose of this study is trying to introduce the photoelectric sensors in the practical application by improving their structure and location. The newly developed sensors are called TEPS (Tube Embraced Photoelectric Sensor), which is located on the liquid distribution lines of the evaporator. In this study, ten TEPSs from four different groups are located on an ASHP unit, which has a nominal heating capacity of 60kW. Experiments are carried out in a

controlled environmental chamber, built following the Chinese standard GB/T 18430.1-2001 (the counterpart of standard ARI 550/590-1998). The characteristics of TEPSs are investigated during periodical frost and defrost cycles. Compared with the original defrost control strategy used by the manufacturer, TEPSs indicate convincible ability to control the defrost operation for ASHP units efficiently.

2 EXPERIMENTAL SYSTEM

2.1 Experimental Apparatus

Experiments are conducted in a controlled environmental chamber, with sizes of 8.2m×7.0m×6.0m (length×width×height). It is built on the purpose to evaluate the performance of commercial size ASHP units in the ranges of heating capacity 55kW to 350kW, cooling capacity 50kW to 300kW, power consumption 20kW to 120kW and air flow rate 8.6 m^3h^{-1} to 52m^3h^{-1}. The discrepancies of test conditions can be controlled within the ranges of ±0.50°C for water temperature, ±1.0°C for dry-bulb temperature, and ±0.50°C for wet-bulb temperature. Fig 1 shows the experimental system in the controlled environmental chamber. An ASHP with nominal heating capacity of 60kW is applied in the test. It consists of two separate units: unit one and unit two. Both of them share a water cooled condenser. Two fin-tube heat exchangers are placed in a V-type form. Each heat exchanger equips a 3-row, 4-circuit coil with 15 distribution lines. The outer diameters of the copper tubes are 10mm for the heat exchanger and 6mm for the distribution lines. Each unit is equipped with a reciprocating compressor with R-22 as the refrigerant, and a four-way reversing valve, which enables the units to defrost separately in reverse cycle.

The refrigerant circuit and hot water supply system are instrumented with PT100 thermocouples to monitor the variation of temperature. The humidity of the air is measured by a humidity sensor VAISALA HMT100 with an accuracy of ±1.7%. Pressure transducers JYB-KO-PAG are placed in the refrigerant lines near the thermocouples to monitor the variation of pressures. A power sensor YOKOGAWA WT-230 with the range of 15V to 600V, 0.5A to 20A and 0.5KHZ to 100KHZ is used to monitor the power input. A water flow-meter AE204MG is used to collect the flow rate variation of hot water supply with an accuracy of ±0.1% in the range of 0ms^{-1} to 10ms^{-1}. A driver card is developed to drive the TEPSs with current and then collected the output voltage from them. Data collected from above sensors can be sent to a computer via a data acquisition switch unit automatically. A digital camera (Canon A1100, 12 megapixels) is applied to capture the images of the heat exchanger under frost condition. The detail information about the instruments is presented in Table 1.

2.2 TEPS

For the typical fin space is 8-10 FPC (Fins Per Centimeter), it is not suitable to locate a photo-electric sensor between fins. Also, it is not easy to set the emitter and receiver on a line of sight for long distance; little deviation will lead to large discrepancy to the results. Therefore, locating the emitter and receiver separately along the fins is not preferred. In this study, by improving the original structure and location of the original photoelectric sensor, a new type of sensor, referred as Tube Embraced Photoelectric Sensor (TEPS) is proposed. As shown in Fig.2, each TEPS consists of a photoelectric sensor, circuit board, connection frame and test section. The circuit board serves as the medium between TEPS and driver card. It provides current to the emitter while transfers output voltage to the driver card. The connection frame is the main structure for TEPSs, which ensures each two sensors embraced together with the tube. The test section is made of heat transfer material, like aluminum or copper. To make it firmly contact with the tube, the test section is embedded in the connection frame, and the bond between the test section and tube is filled with thermal conductive silicone. Thus, frost accumulating on the test surface can be easily monitored by

the TEPS in practical operations. It should be noted that frost growth on the test surface is only similar, but not identical to the heat exchanger surface. To overcome this problem, a structural parameter called initial position is applied to adjust the discrepancy of frost growth speed on the test surface and heat exchanger. As shown in Fig 2 a), the initial position is related to the upper limit of the tested value for frost height. In Table 2, 10 sensors in 4 groups with different initial positions are designed and tested in this study. As revealed in Fig 2 c), every two TEPSs are coupled together on the inlet of distribution line. Owing to the same operating conditions, the frost conditions of unit one and unit two are similar. Thus, these TEPSs are only set on unit one in this study.

2.3 Test Procedure

The experiments are conducted in the standard frost and defrost test conditions of dry bulb and wet bulb temperature at 2°C and 1°C respectively, and hot water inlet temperature is controlled at 40°C with a constant flow rate of $10m^3h^{-1}$. These conditions are stipulated by Chinese standard GB/T 19232-2003. At the initial period, the test conditions in the environmental chamber are built by balancing heat gain with cooling load. After this period, repeatable frost-defrost cycles are obtained. Two units can defrost alternately, one stops operating while the other is in the defrost cycle. The units defrost by the demand of their own strategy. This complex defrost strategy is developed by the manufacturer with the original aim to defrost on demand. The initiation of a defrost cycle is determined by following parameters:

1) Fin temperature,
2) Variation of fin temperature,
3) Environmental temperature, and
4) Time for heating cycle.

The termination of a defrost cycle is decided when the fin temperature reaches 15°C. Although this defrost strategy is well designed, it is still based on monitoring the conditions for frost formation. So, the mal-defrost phenomena always happen in practical applications.

To evaluate the potential improvement for TEPS in periodical frost-defrost cycles, the output voltages of 10 TEPS sensors are monitored every 5s. Data used in evaluating the heating capacity and the power input of the heat pump are integrated across the data collection period to determine overall performance. Three operating characteristics are used to measure the overall defrost performance: numbers of frost-defrost cycles, heating efficiency and the coefficient of performance (COP). Definitely, in a certain heating period, the total heating energy gained by users with several defrost cycles is less than the one without any defrost cycles. So, heating efficiency is defined as Eq. (1):

Where η is the heating efficiency during a heating period. It is applied to evaluate the available heating quantities gained by users in the period with several defrost cycles. Q_{DF} is the efficient heating energy gained by the users in the heating period with several defrost cycles. While Q_{NF} is the heating energy in the same heating period with no defrost cycles. Q_{NF} can be calculated by supposing that defrost cycles to be totally substituted by the heating cycles.

The integrated cyclic COP is defined as the ratio of the integrated heating capacity over the integrated energy consumption. Heating capacity is calculated using the water flow rate and temperature difference between water inlet and outlet in the hot water cycle system as shown in Eq. (2):

COP is calculated as Eq. (3):

Where m is the water flow rate, Δt is the temperature difference between the water inlet and outlet in the hot water cycle system, and W is the electrical power consumption of running the units, including the power of compressors and fans.

3 RESULTS AND DISCUSSION

3.1 Operating Characteristics

The operating characteristics of the tested units are presented in Fig 3 to Fig 7. As shown in Fig 3, experiments are carried out more than 4 hours, including 1 hour for reaching the desirable test condition, which is 2°C for dry bulb temperature and 1°C for wet bulb temperature. These conditions are maintained stable during the test period with little discrepancies in defrost cycles.

Suction and discharge temperatures of the compressor in unit one and two are revealed in Fig 4. It clearly illustrates the numbers of defrost cycles for each unit. Take the data around 90thmin as an example, although large fluctuations for the suction and discharge temperatures are found for both unit one and two, we can easily determine that only unit one defrost, but unit two just stop at this moment. This is acquired by the gap between the suction and discharge temperatures at the moment. During defrost cycles, compressor discharge temperature drops quickly from 80°C to 40°C while the suction temperature increases from -2°C to 30°C. Two units defrost alternately. For unit one, five defrost cycles initiate at the 30thmin, 90thmin, 125thmin, 185thmin and 230thmin, while for unit two, four defrost cycles initiate at the 35thmin, 120thmin, 180thmin and 245thmin. There are totally nine times of frost-defrost cycles during the test period 260min. Based on these results, the average defrost interval for the test ASHP units is 28.8 min.

As shown in Fig 5, both the outlet and inlet water temperature of condenser keeps relatively stable at 45°C and 40°C in the heating cycles. However, in the defrost cycles, the outlet temperature drops quickly from 45°C to 38°C. At the end of defrost cycle, the outlet water temperature drops even lower than the inlet water temperature. Correspondingly, heating capacity drops quickly as shown in Fig 6. This means units will take energy from the water loop, which leads to a negative heating quantity gained by the users, additional heating load added to the next heating cycle, and further adverse impacts exerted on the heating effect for users.

In addition, it should be noted in Fig 6, though frost has accumulated on the surface of heat exchanger, the heating capacity and energy consumption of the units can keep stable at 58kW and 18kW. The reason for this is that the frost is not very heavy. Fig 7 presents the frosting images on the edge of fins when defrost cycles initiate. The images at the 30thmin, 35thmin and 120thmin reveal that there is only small amount of frost accumulating on the heat exchanger. The defrost operations are not appropriate. Though heavier frost appears at the 90thmin, 180thmin and 230thmin**,** the typical frost thicknesses at these moments are only around 0.5mm. Frost exerts little effect on the performance of the ASHP. So, it is still not necessary to defrost. By illustrating the variation of COP, Fig 8 further confirms that mal-defrosts happen in these cycles. It reveals that COP can always keep stable at 3.2 even at the beginning of defrost cycles. These mal-defrost controls lead to frequent operation of defrost, which accompanies unnecessary heating lost and lower heating efficiency. Therefore, to improve the heating efficiency, defrost interval should be extended to avoid frequent defrost operations.

3.2 Output Voltage Of TEPS

Fig 9 reveals the output voltages of 4 groups of TEPSs. In Fig 9 a) to c), the output voltage increases with the frost growth and decreases quickly corresponding to the defrost cycle. It demonstrates that these TEPSs are sensitive to the variation of the frost. According to the previous study (J. Xiao and W. Wang et al., 2009), the response output voltage for initiating the defrost control is 9.0V. Fig 9 a) to Fig 9 c) indicates that at the 30thmin, the output voltages from the first three groups are just around 4.0V, 6.0V and 7.0V respectively. They are far away from the response value 9.0V. So, if controlled by the TEPS, unit one will not defrost at this moment. Based on the same argument, the defrost control at the 125thmin for unit one is not necessary. Since the two units operate under similar conditions, it is reasonable to conclude that the defrost controls for unit two at the 35thmin, 120thmin are also not necessary. In this way, the total numbers of defrost cycles can be reduced from 9 to 5, large amount of mal-defrost controls are avoided, and the average defrost interval can be prolonged to 52min. In addition, the output voltages of TEPSs at the 90 thmin, 180thmin and 230thmin are just 8.7V, 8.8V and 8.9V. None of them reach the response value of 9.0V. This means that the defrost intervals can be extended by TEPS. By prolonging the data along with their trend curves, the supposed initiation points of the defrost cycles, A, B and C for group I, II and III are obtained. These results indicate that the average defrost interval can be even longer than 52min. Confidently, there is no less than 80% improvement compared with the original strategy of 28.8min. Therefore, TESP is helpful for the units to avoid frequent defrost in undesirable conditions.

However, in Fig 9 d), the initial output voltages of Group IV do not start at 0V and they can get the response value of 9.0V quickly. These unexpected results figure out that Group IV is not suitable in practical application for monitoring the frost height. The reason for this is that the initial position of this group is only 0.4mm, which leads to the optical passage partly blocked by the test section. The frost height available to be monitored by the TEPS is limited in a little value. Therefore, to provide enough space for the growth of frost, the initial position of TEPS needs to be higher than 0.4mm.

3.3 Energy Efficiency Improvement Of TEPS

Calculated from the data in Fig 6, the efficient heating energy Q_{DF} during the test period is 597.7 MJ. In each defrost cycle, the average heating energy lost is 14.2 MJ, and energy consumption is 3.81 MJ. In the supposing conditions with no defrost cycles, the total heating capacity Q_{NF} is 726 MJ. Thus, the heating efficiency of the original defrost control strategy is 82.2%. Fig. 10 presents the heating efficiency and COP under different defrost intervals. As stated in section 3.2, the total numbers of defrost cycles can be confidently reduced to no more than 5 times by application of TEPS. The defrost interval is no less than 52min correspondingly. Referring to Fig.10, the heating efficiency at this moment will achieve 90.2%, which has 8.0% of improvement to the original one. And the COP will increase from 2.38 to 2.58, also with 8% improvement. These results reveal that the energy efficiency of the units will be definitely improved no less than 8.0% by introducing TEPSs into defrost controls.

4 CONCLUSION

An innovative “Tube Embraced Photoelectric Sensor” (TEPS) is proposed in this paper with the aim to improve the practical ability of the photoelectric sensor in defrost control. To investigate the characteristics of the presented sensor and further to evaluate its improvement in heating efficiency and energy consumption, experiments are carried out in an environmental chamber with an air source heat pump of 60kW nominal heat capacity. The conclusions are as follows.

1) By monitoring the frost directly and accurately, TEPS can prolong the defrost interval and reduce the numbers of undesirable defrost controls for ASHP units. Results indicate that the

numbers of defrost control by TEPS can be definitely reduced from 9 to 5 in 260min, no less than 80% improvement compared with the original strategy. This enables ASHP units to defrost in accordance with their own demand.
2) TEPSs with an initial position higher than 0.4mm prove to be efficient in monitoring frost growth due to their special structure and location. Lower values for the initial position are found unsuitable to the practical application,
3) By reducing the numbers of defrost controls, both heating efficiency and COP of the tested ASHP units can be enhanced. In this study, there is evidently 8% of improvement in the heating efficiency and COP.
Though TEPS exhibits excellent characteristics in the defrost control, ongoing work still needs to study the structure parameters of TEPS and then develop corresponding optimal defrost control strategy.

ACKONWLEDGEMENT

This work was supported in part by the National Natural Science Foundation of China (Grant no. 50708002) and with additional support of the Beijing Municipality Key Lab of Heating, Gas Supply, Ventilating and Air Conditioning Engineering (KF201005). The authors are grateful for the support of these sponsors.

5 TABLES, FIGURES AND EQUATIONS

Table 1: Information of the experiment instrumentation

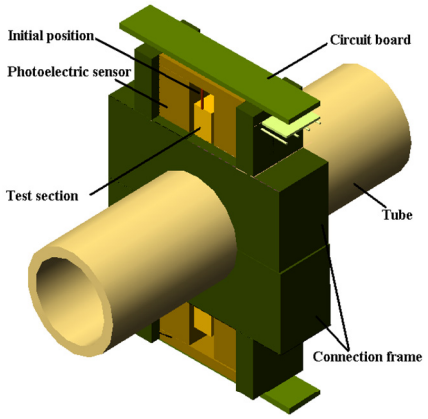
Device	Number	Accuracy of Reading	Full Scale	Model
Flow-meter	1	±0.1%	0~10ms^{-1}	AE204MG
Power sensor	1	±0.1%	15~600V 0.5~20A 0.5~100kHZ	YOKOGAWA WT-230
Temperature Sensor	8	±0.5^{o}C	-20~55°C	CHINO PT100
Humidity sensor	1	±1.7%RH	0~100%RH	VAISALA HMT100
Pressure sensor	4	±0.25%	0~1MPa, 0~4MPa	JYB-KO-PAG
Driver Card	1		5mA, 10mA, 15mA, 20mA	
Digital camera	1			Canon A1100
Data Acquisition/ Switch Unit	1	0.004%DV		Agilent-34970A

Table 2: Information of tested TEPS sensors

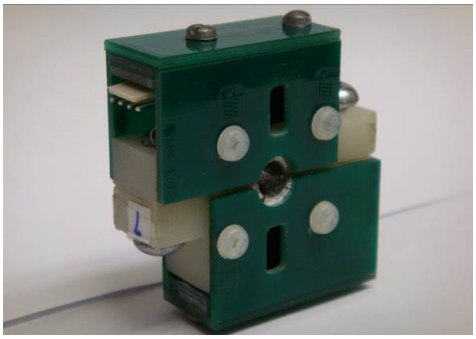
Group	Number	Serial Number	Initial Position (mm)
Group I	4	1#, 2#, 3# and 4#	1.0
Group II	2	5# and 6#	0.8
Group III	2	7# and 8#	0.6
Group IV	2	9# and 10#	0.4



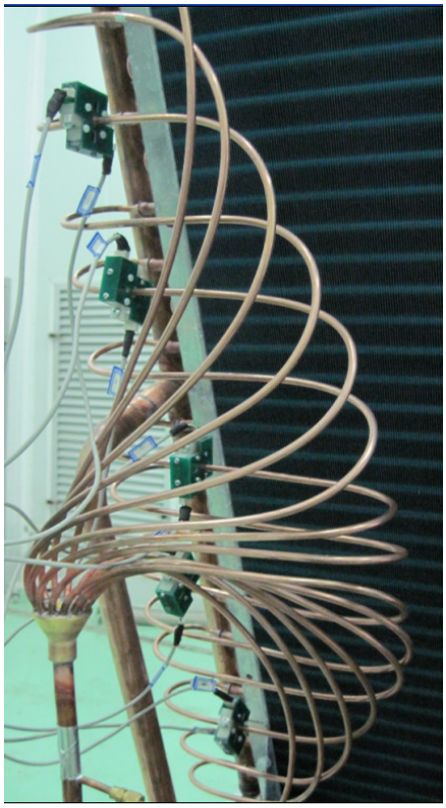
Figure 1: Experimental system



a) Schematic of TEPS



b) TEPS



c) Location of TEPS

Figure 2: TEPS information

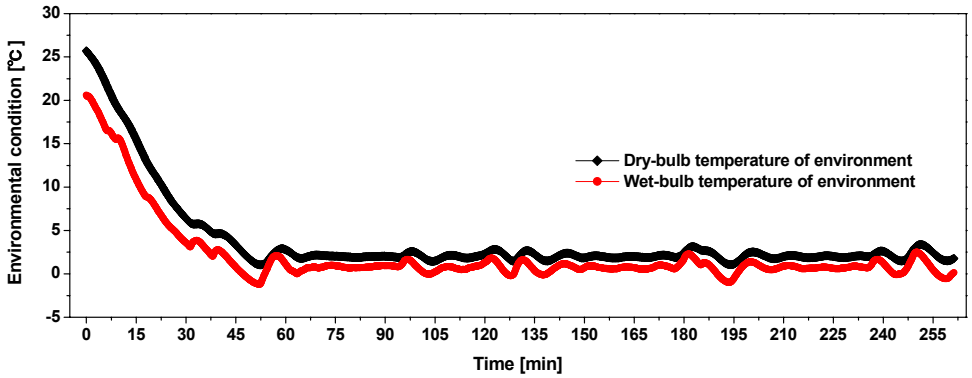
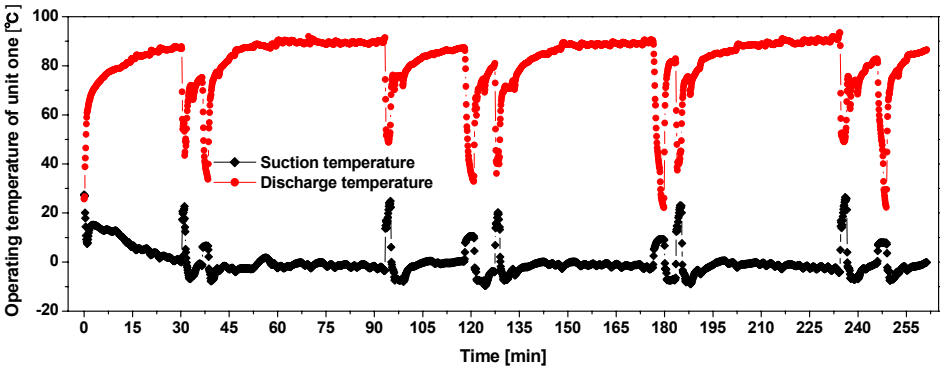
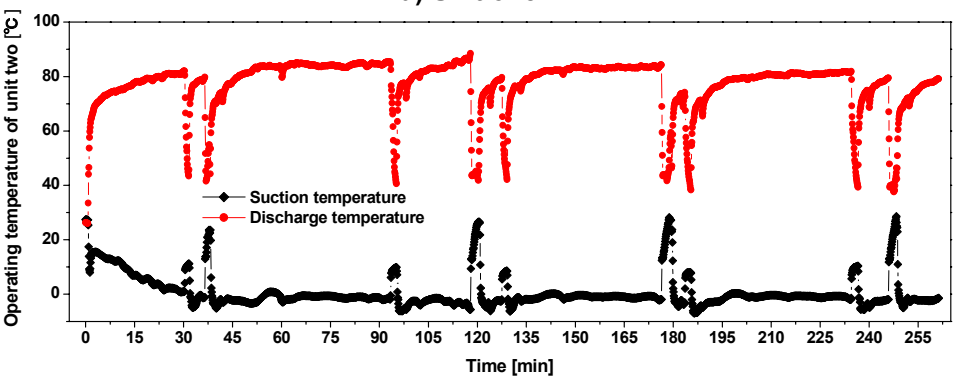


Figure 3: Test conditions



a) Unit one



b) Unit two

Figure 4: Suction and discharge temperature

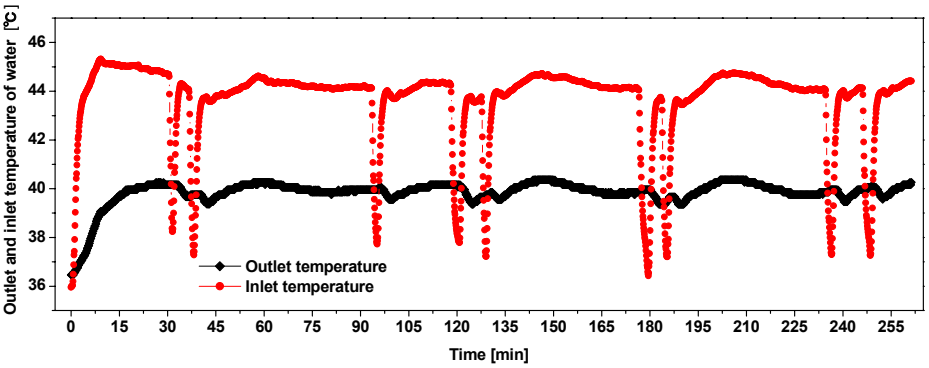


Figure 5: Inlet and outlet hot water temperature

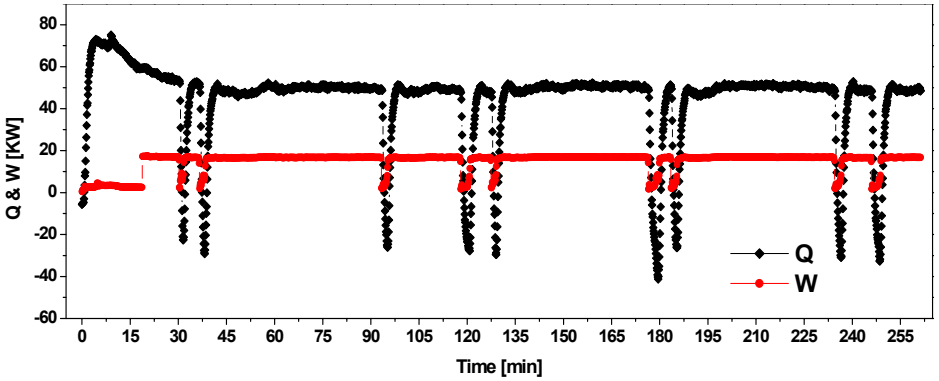


Figure 6: Heating capacity and power consumption of the units

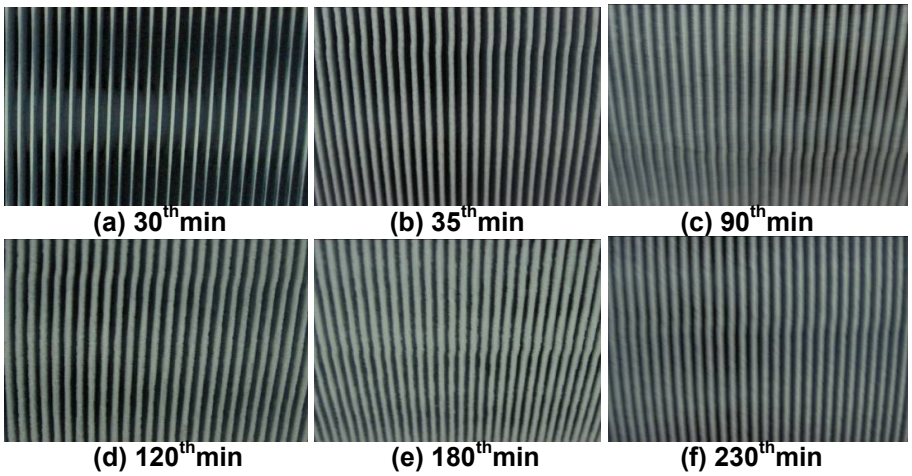


Figure 7: Frost condition before defrost cycle

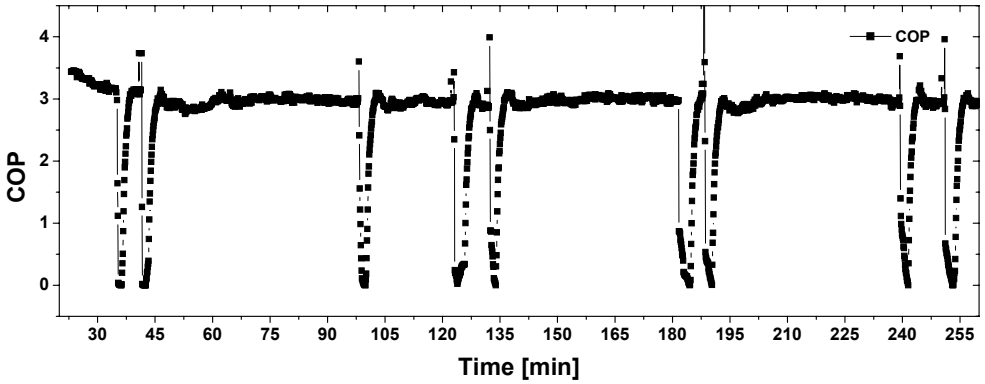
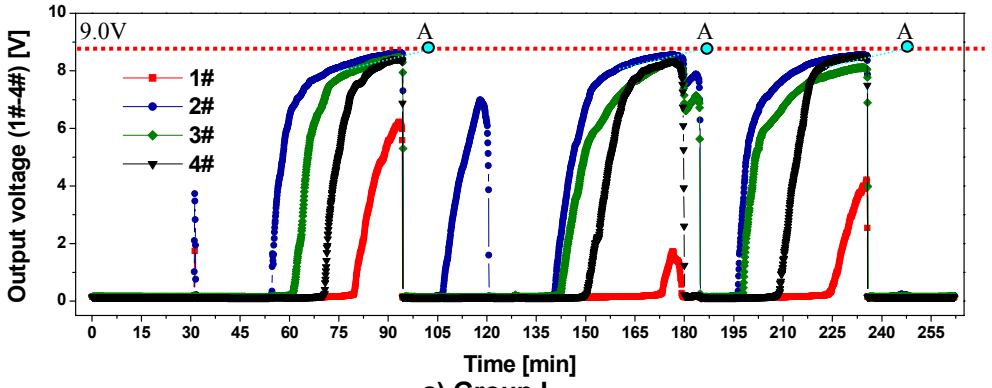
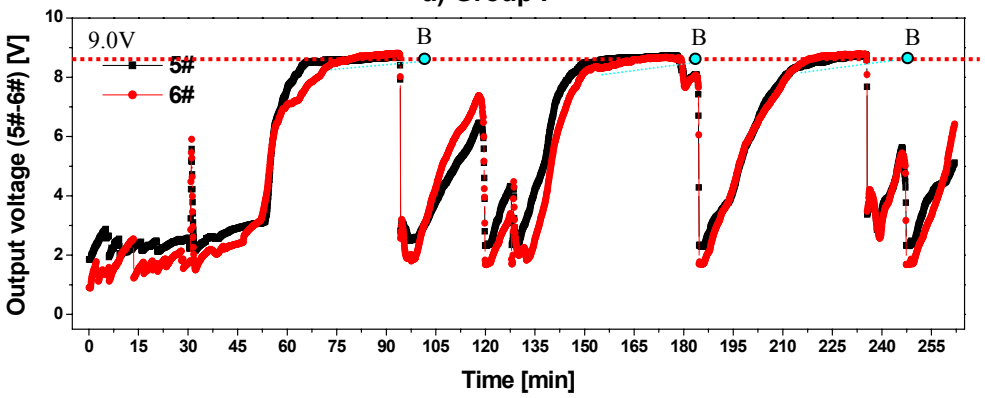


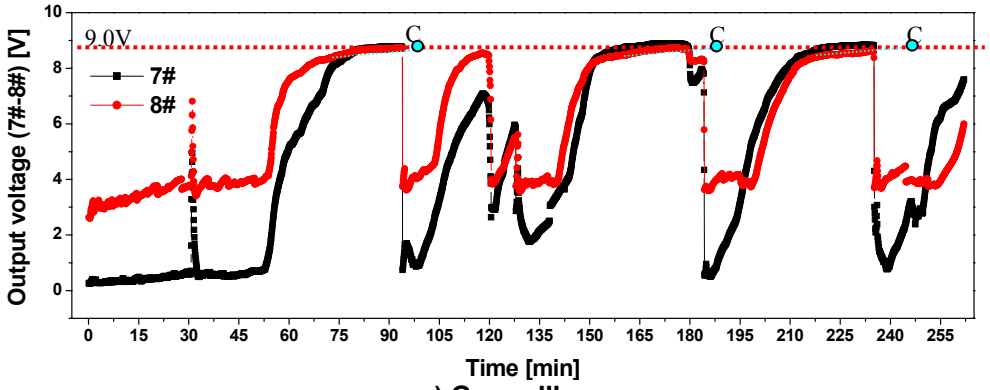
Figure 8: Variation of COP



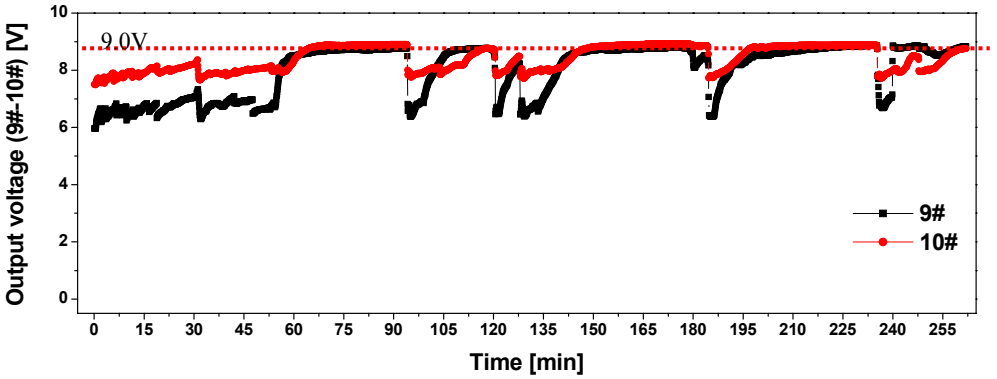
a) Group I



b) Group II



c) Group III



d) Group IV

Fig 9: Output voltage of photoelectric sensors

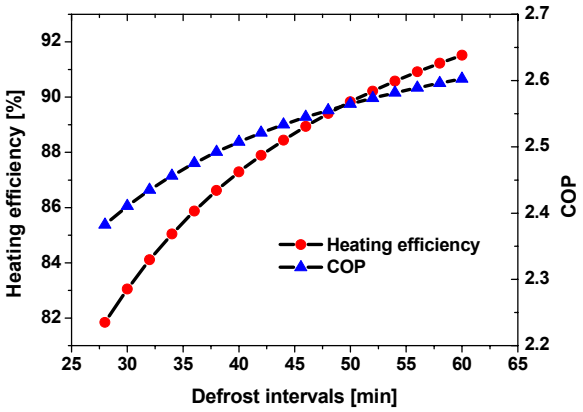


Figure 10: Heating efficiency and COP with different defrost intervals

$$\eta = Q_{DF} / Q_{NF} \leq 1 \tag{1}$$

η — Heating efficiency
Q_{DF} — Effective heating capacity with several defrost cycles, W
Q_{NF} — Heating capacity without defrost cycles, W

$$Q_{DF} = mc_p \Delta t \tag{2}$$

m — Water mass flow rate, kgs^{-1}
c_p — Specific heat at constant pressure, $Jkg^{-1}K^{-1}$
Δt — Temperature difference between supply and return water, °C

$$COP = Q_{DF} / W \tag{3}$$

W — Input electrical power, W

6 REFERENCES

Byun, J.S., Jeon, C.D., Jung, J.H., and Lee, J. 2006. “The application of photo-coupler for frost detecting in an air-source heat pump”, *International Journal of Refrigeration*, Vol. 29, pp. 191–198.

Ciricillo, S.F. 1985. “Heat pump de-icing/controlling for energy conservation and costs”, Proceedings of the Clima 2000 Congress on Heating, Ventilation and Air Conditioning, Copenhagen, pp. 87–92.

Datta, D., Tassou, S.A. 1999. “Defrost control of evaporator coils using artificial intelligence techniques”, Proceedings of the 20th International Conference of Refrigeration, IIR/IIF, Sydney, Australia, pp. 118.

Datta, D., Tassou, S.A. 2002. “Implementation of a defrost on demand control strategy on a retail display cabinet”, Proceedings IIF-IIR-Commission D1/B1-Urbana, Illinois, USA, pp. 218–226.

Heinzen, R.A. 1988. “How adaptive defrost maintains refrigeration system efficiency”, *Australian Institute of Refrigeration Air Conditioning and Heating*, Vol. 42, pp. 12–16.

Lawrence, J.M.W., and Evans, J.A. 2008. “Refrigerant flow instability as a means to predict the need for defrosting the evaporator in a retail display freezer cabinet”, *International Journal of Refrigeration*, Vol. 31, pp. 107-112.

Lenic, K., Trp, A., and Frankovic, B. 2009. “Prediction of an effective cooling output of the fin-and-tube heat exchanger under frosting conditions”, *Applied Thermal Engineering*, Vol. 29, pp. 2534–2543.

Llewelyn, D.S. 1984. “A significant advance in defrost control”, *International Journal of Refrigeration*, Vol. 7, pp. 334–335.

Muller, E.D. 1975. “A new concept for defrosting refrigeration plants”, *Kalte*, Vol. 28, pp. 52-54.

O’Neal, D.L., Peterson, K.T.1991. “Effect of short-tube orifice size on the performance of an air source heat pump during the reverse-cycle defrost”, *International Journal of Refrigeration*, Vol. 14, pp. 52-57.

Paone, N., Rossi, G. 1991. “Fiber-optic ice sensors for refrigerators”, Proceedings of SPIE 1511, pp. 129–139.

Thybo, T., Rasmussen, B.D., and Izadi-Zamanabadi, R. 2002. “Detecting air circulation faults in refrigerated display cabinets”, Proceedings IIF-IIR-Commission D1/B1-Urbana, Illinois, USA, pp. 211–217.

Woodley, C.B.C. 1989. “Saving on the defrost”, *Air Conditioning Refrigeration News*, August, pp. 62.

Xiao, J., Wang, W., Zhao, Y.H., and Zhang, F.R. 2009. “Analysis of the feasibility and characteristics of photoelectric technique applied in defrost-control”, *International Journal of Refrigeration*, Vol. 32, pp. 1350–1357.